

## Genome-wide interaction analysis of pathological hallmarks in Alzheimer's disease



Hui Wang<sup>a</sup>, Jingyun Yang<sup>b,c</sup>, Julie A. Schneider<sup>b,c,d</sup>, Philip L. De Jager<sup>e,f</sup>,  
David A. Bennett<sup>b,c,\*\*</sup>, Hong-Yu Zhang<sup>a,\*</sup>

<sup>a</sup>Hubei Key Laboratory of Agricultural Bioinformatics, College of Informatics, Huazhong Agricultural University, Wuhan, Hubei, China

<sup>b</sup>Rush Alzheimer's Disease Center, Rush University Medical Center, Chicago, IL, USA

<sup>c</sup>Department of Neurological Sciences, Rush University Medical Center, Chicago, IL, USA

<sup>d</sup>Department of Pathology, Rush University Medical Center, Chicago, IL, USA

<sup>e</sup>Center for Translational and Computational Neuroimmunology, Columbia University Medical Center, New York, NY, USA

<sup>f</sup>Cell Circuits Program, Broad Institute, Cambridge, MA, USA

### ARTICLE INFO

#### Article history:

Received 14 August 2019

Received in revised form 21 April 2020

Accepted 22 April 2020

Available online 29 April 2020

#### Keywords:

Alzheimer's disease

Tau

Amyloid- $\beta$

Epistasis

### ABSTRACT

Genome-wide association studies have identified many loci associated with Alzheimer's dementia. However, these variants only explain part of the heritability of Alzheimer's disease (AD). As genetic epistasis can be a major contributor to the “missing heritability” of AD, we conducted genome-wide epistasis screening for AD pathologies in 2 independent cohorts. First, we performed a genome-wide epistasis study of AD-related brain pathologies ( $N_{\max} = 1318$ ) in ROS/MAP. Candidate interactions were validated using cerebrospinal fluid biomarkers of AD in ADNI ( $N_{\max} = 1128$ ). Further functional analysis tested the association of candidate interactions with neuroimaging phenotypes. For tau and amyloid- $\beta$  pathology, we identified 2803 and 464 candidate SNP-SNP interactions, respectively. Associations of candidate SNP-SNP interactions with brain volume and white matter changes from neuroimages provides additional insights into their molecular functions. Transcriptional analysis supported possible gene-gene interactions identified by statistical screening through their co-expression in the brain. In summary, we outlined an exhaustive epistasis analysis to identify novel genetic interactions with potential roles in AD pathologies. We further delved into the functional relevance of candidate interactions by association with neuroimaging phenotypes and analysis of co-expression between corresponding gene pairs.

© 2020 Elsevier Inc. All rights reserved.

### 1. Introduction

The genetic architecture underlying Alzheimer's disease (AD) is complex. For the familial form of AD, which only accounts for 1%–5% of AD, mutations in *APP*, *PSEN1*, and *PSEN2* usually guarantee early onset of AD (Tanzi, 2012). By contrast, large-scale genome-wide association studies identified common variants with small effects for Alzheimer's dementia (Lambert et al., 2013). Yet, the complete genetic architecture for late-onset AD remains elusive. It is estimated that about a quarter of the phenotypic variance for late-onset AD can be explained by *APOE* combined with common variants (Lee

et al., 2013; Ridge et al., 2013); this value is considerably lower than the estimated two-thirds of heritability from twin studies (Gatz et al., 2006). It has been proposed that epistasis, which refers to the departure from “independence” of the effects of different genetic loci in the way that they combine to cause disease, can help explain some of the “missing heritability” (Raghavan and Tosto, 2017). Therefore, in this study, we investigated the genetic interactions for Alzheimer's pathology to unravel novel genetic mechanisms missed by traditional genome-wide association studies.

Previous work on epistasis in AD mainly focused on specific gene pair interactions supported by prior biological evidence. For example, proinflammatory interleukin-6 (IL-6) level is relatively higher in patients with AD and the anti-inflammatory interleukin-10 (IL-10) level is relatively lower in patients with AD (Remarque et al., 2001). Subsequently, the genetic interactions between IL-6 and IL-10 were reported in a recent study by measuring the synergy factor (1.69,  $p = 0.01$ ) (Combarros et al., 2009b). Moreover, elevated iron levels in patients with AD spurred an interest in the

\* Corresponding author at: Huazhong Agricultural University, No. 1 Shizishan Street, Hongshan District, Wuhan, Hubei 430070, China. Tel.: +86-27-87285085; fax: +86-27-87280877.

\*\* Corresponding author at: Rush Medical College, 600 S Paulina St, Chicago, IL 60612, USA. Tel: +1-312-942-4463; fax: +1-312-942-4154.

E-mail addresses: [David\\_A\\_Bennett@rush.edu](mailto:David_A_Bennett@rush.edu) (D.A. Bennett), [zhy630@mail.hzau.edu.cn](mailto:zhy630@mail.hzau.edu.cn) (H.-Y. Zhang).

discovery of potential interactions in iron metabolism. As a result, the interaction between hemochromatosis gene (*HFE*) and transferrin gene (*TF*) was identified and replicated by subsequent studies (Kauwe et al., 2010; Robson et al., 2004).

To identify novel genes and genetic interactions for AD susceptibility, it is necessary to screen epistasis on a genome-wide scale. However, there are major challenges to screening statistical epistasis through the genome. First, statistical epistasis appearing in one data set usually cannot be replicated in another data set. For example, one study of more than 100 possible epistasis pairs reported in previous studies could only replicate 27 pairs in their own data (Combarros et al., 2009a). Second, the stringent *p* value required for significance resulting from adjusting for multiple hypothesis tests often cannot be attained (Murk and DeWan, 2016). In addition, exhaustive screening of all possible epistasis is computationally intensive. Even for fast screening methods, such as “Boolean Operation-based Screening and Testing”, nearly 60 hrs are required to evaluate  $6.5 \times 10^{10}$  interactions between 360,000 SNPs on a standard 3.0 GHz computer with 4G memory (Wan et al., 2010). On a genome-wide scale, there has been only 2 replicated genetic interactions reported to be associated with Alzheimer's dementia. One is the interaction between rs6455128 (*KHDRBS2*) and rs7989332 (*CRYL1*) which was discovered in a French cohort and replicated in another cohort from Germany (Gusareva et al., 2014). In a recent study, the interaction between rs3733980 (*WWC1*) and rs7175766 (*TLN2*) that was associated with AD in males was identified and validated by Drosophila eye experiments (Gusareva et al., 2018).

To solve the aforementioned problems in the genome-wide interaction analysis (Gusareva et al., 2014), we conducted epistasis screening in 2 stages and validated epistasis in another independent data set. More importantly, we leveraged neuropathologic endophenotypes which have greater power for genetic associations (Bennett et al., 2009). During the first stage, possible SNP-SNP interactions for AD-related neuropathology in The Religious Orders Study and Rush Memory and Aging Project (ROS/MAP) were filtered using a simple linear regression model. We reported all candidate SNP-SNP interactions that passed a less conservative correction accounting for the total number of tests performed in second stage. After the 2-stage analysis, validation of candidate SNP-SNP interactions was evaluated on a subset of samples from The Alzheimer's Disease Neuroimaging Initiative (ADNI) with cerebrospinal fluid (CSF) biomarkers of AD measured. Furthermore, candidate gene-gene interactions mapped by the SNPs were ranked by their co-expression in the brain. As a result, credible interactions contributing to AD pathology were discovered and validated by multiple sources.

## 2. Methods

### 2.1. Study subjects

ROS/MAP are longitudinal clinical-pathologic cohort studies of aging and dementia (Bennett et al., 2018). The diagnosis of Alzheimer's dementia for each subject was obtained from a neurologist by reviewing all available clinical data at the time of death, blinded to postmortem data. Amyloid- $\beta$  ( $A\beta$ ) and tau neuropathology were measured using immunohistochemistry and automated image processing for total amyloid and paired helical filament tau (PHF-tau), and a modified Bielschowsky silver staining technique for neuritic plaques, diffuse plaques, and neurofibrillary tangles (see Supplementary Method). A total of 2090 individuals in ROS/MAP have been genotyped in 2 batches, of which 1374 individuals received clinical consensus diagnosis of cognitive status (no/mild cognitive impairment or Alzheimer's dementia). Of 1579 autopsied

persons at the time of these analyses, 1326 had genotype data, of which 1318 individuals had either one of 5 pathological measurements that passed quality control. Of the 1318 individuals, 1316 had neurofibrillary tangles, neuritic plaques, and diffuse plaques measured, 1285 had total PHF-tau measured, and 1276 had total amyloid measured.

ADNI (including phases 1, GO, and 2) is an international cooperative study to investigate the biomarkers of AD and develop treatment to slow or stop Alzheimer's dementia progression (Petersen et al., 2010). All subjects were administered clinical evaluations at the time of enrollment by expert physicians. CSF total tau (T-tau), phosphorylated tau (P-tau), and  $\beta$ -amyloid (1–42) ( $A\beta_{1-42}$ ) levels were measured by the electrochemiluminescence immunoassays (see Supplementary Method). There are 1550 genotyped individuals with a diagnosis of Alzheimer's dementia in ADNI, of which 1128 individuals had either one of the 3 CSF biomarkers that passed quality control. Of the 1128 individuals, 1127 had CSF T-tau and P-tau measured, 1128 had CSF  $A\beta_{1-42}$  measured. Characteristics of the study participants for ROS/MAP (N = 2090) and ADNI (N = 1550) are summarized in Table 1.

### 2.2. Molecular and structural neuroimaging

For ADNI, molecular and structural neuroimaging data were generated. A total of 855 individuals underwent structural magnetic resonance imaging protocols to generate estimates of entorhinal cortex and hippocampal volume. To generate estimates of fractional anisotropy (FA) for 5 bilateral fronto-temporal-occipital and interhemispheric white matter tracts (sagittal stratum, hippocampal segment of cingulum bundle, splenium of corpus callosum, inferior fronto-occipital fasciculus, and superior longitudinal fasciculus) implicated in AD, diffusion tensor volumes were first obtained from diffusion-weighted images. Based on diffusion tensor volumes, estimates of FA across the 5 brain regions were generated for 216 subjects.

### 2.3. Genotyping and imputation

A total of 1708 individuals in ROS/MAP were genotyped using the Affymetrix GeneChip 6.0 (Affymetrix, Inc, Santa Clara, CA, USA) at the Broad Institute's Center for Genotype or the Translational Genomics Research Institute. An additional batch in ROS/MAP was

**Table 1**  
Characteristics of study participants from ROS/MAP (N = 2090) and ADNI1/GO/2 (N = 1550)

ROS/MAP	AD (n = 568)	Non-AD (n = 1522)	Diff ( <i>p</i> ) <sup>a</sup>
Sex (F/M)	392 F, 176 M	1067 F, 455M	0.63
Age at death, y (SD)	90.92 (5.89)	88.09 (6.72)	<0.0001
Education, y (SD)	16.22 (3.66)	16.34 (3.51)	0.49
MMSE (SD)	12.69 (8.55)	26.33 (4.39)	<0.0001
<i>APOE</i> $\epsilon$ 4 status (-/+)	-382, +186 (0.33)	-1232, +290 (0.19)	<0.0001
ADNI	AD (n = 599)	Non-AD (n = 951)	Diff ( <i>p</i> ) <sup>a</sup>
Sex (F/M)	253 F, 346 M	423 F, 528M	0.4
Age at AD, y (SD)	74.71 (8.12)	77.22 (7.40)	<0.0001
Education, y (SD)	14.79 (4.64)	15.99 (3.26)	<0.0001
MMSE (SD)	22.19 (5.63)	28.35 (2.30)	<0.0001
<i>APOE</i> $\epsilon$ 4 status (-/+)	-220, +379 (0.63)	-629, +322 (0.34)	<0.0001

Key: AD, Alzheimer's disease; ADNI, Alzheimer's Disease Neuroimaging Initiative; Age at AD, age when developed AD for ADs or age at last valid record for non-ADs; *APOE*  $\epsilon$ 4 status (-/+), presence of  $\epsilon$ 4 allele; Diff, statistical difference between AD and non-AD; F, female; M, male; MMSE, Mini-Mental Status Examination score; ROS/MAP, The Religious Orders Study/the Rush Memory and Aging Project; SD, standard deviation.

<sup>a</sup> *p* values are calculated by Fisher's exact tests (for sex and *APOE*  $\epsilon$ 4 status) or two-sample t-tests (for age at death, age at AD, education and MMSE).

generated on 382 individuals using the Illumina HumanOmniExpress (Illumina, Inc, San Diego, CA, USA) at the Children's Hospital of Philadelphia. In total, there are 2090 genotyped individuals in ROS/MAP. A total of 757 ADNI1 subjects were genotyped using the Illumina Human610-Quad BeadChip (Illumina, Inc, San Diego, CA, USA). A total of 793 ADNIGO/2 subjects were genotyped using the HumanOmniExpress BeadChip (Illumina Inc, San Diego, CA, USA). In total, there are 1550 genotyped individuals in ADNI.

To merge the 2 batches in ROS/MAP, genotype data for 382 individuals from the second batches were phased using Eagle (v2.4.1) (Loh et al., 2016) and imputed using Minimac3 (v2.0.1) (Das et al., 2016). To validate the SNP-SNP interactions identified by ROS/MAP, genotype data from ADNI1 and ADNIGO/2 subjects were merged after being phased and imputed by the same pipeline. First, the genotyping data were aligned to the human assembly GRCh37/hg19 using UCSC's liftOver tool (Casper et al., 2017). Next, the alleles were checked to match with the GRCh37 reference sequence. Imputation were carried out as described in a previous study (Van Leeuwen et al., 2015), with 1000 Genomes phase3 integrated haplotypes being the reference panel (Consortium et al., 2015). Imputed variants with an imputation quality statistic ( $R^2$ ) below 0.3 were discarded. Furthermore, calls with uncertainty greater than 0.2 or import dosage certainty smaller than 0.8 were treated as missing.

Using subjects in ROS/MAP as the discovery cohort, SNPs were first filtered by Hardy-Weinberg Equilibrium test with a Bonferroni-based nominal significance threshold of  $0.05/714014$  SNPs =  $7.0 \times 10^{-8}$ . Then, SNPs with minor allele frequency  $<0.05$  or missing calling rate  $>0.10$  were removed. In addition, SNPs were linkage disequilibrium (LD) pruned by a window size of 50 bp, window increment of 1 bp, and LD threshold of  $r^2$  0.75. After these steps, 279409 of 714014 variants passed filters and quality control. All aforementioned quality control steps were performed using PLINK (v1.90b4.10) (Chang et al., 2015).

#### 2.4. Epistasis screening methods

For ROS/MAP discovery cohort, epistasis was screened against neurofibrillary tangles, total PHF-tau, neuritic plaques, diffuse plaques, and total amyloid. We removed those SNP-SNP pairs for which there were less than 3 observations in the lowest SNP  $\times$  SNP contingency table cell, which could lead to spurious results. More specifically, only SNP-SNP pairs with a cell size either more than 3 or equal to 0 in each cell of the  $3 \times 3$  genotype matrix were kept for further analysis, resulting in 12,547,471,105 independent SNP-SNP pairs to be evaluated. Therefore, when applying the Bonferroni procedure, our threshold for statistical significance was set to  $\alpha = 3.98 \times 10^{-12}$ . Simple linear regression was used to construct a pool of possible SNP-SNP interactions in the first stage. SNP-SNP interactions with nominal  $p$  values  $<1 \times 10^{-5}$  were selected for further analysis. Epistasis screening were performed using PLINK (Chang et al., 2015) in the first-stage analysis. In the second stage, the genotypic model (see [Supplementary Method](#)) implemented in INTERSNP (Herold et al., 2009), which contains both additive and dominant effects for each SNP and all 4 possible epistasis models, was applied. Rather than the usual 0, 1, 2 coding, which represents the number of minor alleles, Cordell's dominant coding was used to represent the genotype of each SNP in this model (Cordell, 2002). The effects of sex, age (determined by the date of death in ROS/MAP or date of examination in ADNI), and APOE genotype (number of  $\epsilon 4$  alleles) were examined in the model as covariates. Finally, we report all SNP-SNP interactions as "suggestive" that passed a less conservative correction accounting for the total number of pairs analyzed in the second stage. These interaction results may warrant

future investigation and are reported along with significant interactions in the supplementary tables.

SNP-SNP interactions that were identified in the discovery cohort were validated using the CSF biomarkers of AD in ADNI by the genotypic model described previously. The union of candidate interactions for tau-related pathologies (including neurofibrillary tangles and total PHF-tau) were further tested for their association with CSF T-tau and P-tau levels in ADNI. The union of candidate interactions for A $\beta$ -related pathologies (including neuritic plaques, diffuse plaques, and total amyloid) was further tested for their association with CSF A $\beta_{1-42}$  levels in ADNI.  $p$  values were Bonferroni corrected. To avoid spurious interactions caused by long-range LD, SNP-SNP interactions on the same chromosome with an  $R^2 > 0.2$  were filtered out. In addition, to deduce biological epistasis from the statistically significant epistasis, interactions were visualized by plotting the mean value of each cell in a contingency table of  $3 \times 3$  genotype combinations.

#### 2.5. Gene expression analysis

RNA was extracted from the gray matter of the dorsolateral prefrontal cortex of 724 subjects from the ROS/MAP cohorts. These samples were quantified by Nanodrop, and quality was evaluated by Agilent Bioanalyzer (Agilent Technologies, Inc, Santa Clara, CA, USA). A total of 582 RNA-Seq samples met quality (Bioanalyzer RNA integrity score  $>5$ ) and quantity (5ug) thresholds. Then RNA-Seq data were processed by a parallelized and automatic pipeline, which includes trimming the beginning and ending bases from each read, identifying and trimming adapter sequences from reads, detecting and removing rRNA reads, and aligning reads to the reference genome. Nongapped aligner Bowtie was used to align reads to transcriptome reference, and then RNA-Seq by expectation maximization was applied to estimate expression levels for all transcripts. The fragments per kilobase of exon model per million reads mapped were quantile normalized, and the potential batch effects were removed by the combat package in R (see [Supplementary Method](#)).

Co-expression between 2 interacting genes was calculated using Pearson correlation. Gene pairs were obtained by mapping SNPs in the SNP-SNP interactions to the nearest genes within a distance of 10 kb. Genes which were detected (FRKM  $>0$ ) in less than 100 samples were excluded from analysis. After co-expression analysis, gene-gene interactions were ranked by their co-expression  $p$  value.

### 3. Results

#### 3.1. Genome-wide epistasis screening and validation

Genome-wide epistasis screening for neurofibrillary tangles, total PHF-tau, neuritic plaques, diffuse plaques, and total amyloid were carried out in ROS/MAP. First, the Pearson correlation coefficients of 5 measurements were examined (Fig. 1). As expected, measurements of tau neuropathology, neurofibrillary tangles and total PHF-tau, were highly correlated. Measurements of A $\beta$  neuropathology (neuritic plaques, diffuse plaques, and total amyloid) showed moderate correlations. For neurofibrillary tangles and total PHF-tau, a total of 435,358 and 526,204 SNP-SNP interactions met the criterion of a cell size either more than 3 or equal to 0 and a nominal  $P$  threshold of  $1 \times 10^{-5}$  by linear regression in the first stage. In the second stage, 32,960 (neurofibrillary tangles) and 65,263 (total PHF-tau) suggestive SNP-SNP interactions were reported after adjusting for age, sex, and APOE status using a genotypic model that includes both additive and dominant effects, as well as 4 different interaction terms. Among them, 2700 (neurofibrillary tangles) and 9005 (total PHF-tau) SNP-SNP interactions

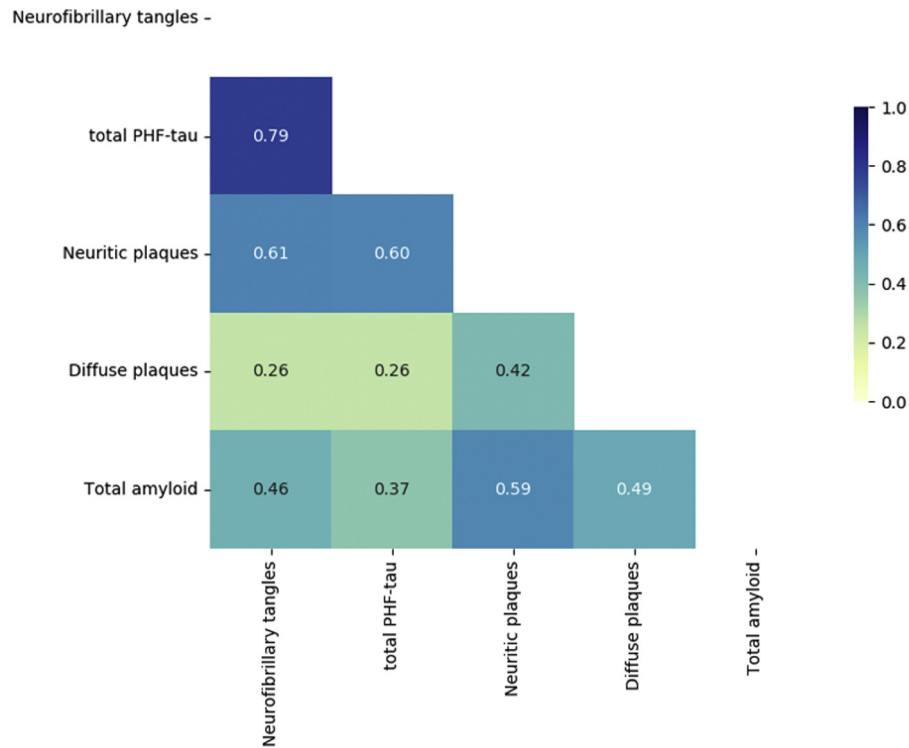


**Fig. 1.** Pair-wise Pearson correlation coefficients of neurofibrillary tangles, total PHF-tau, neuritic plaques, diffuse plaques, and total amyloid in ROS/MAP. Abbreviations: PHF-tau, paired helical filament tau; ROS/MAP, The Religious Orders Study/the Rush Memory and Aging Project.

were significant under a Bonferroni-based nominal significance threshold of  $3.98 \times 10^{-12}$ . For validation, candidate SNP-SNP interactions discovered for neurofibrillary tangles and total PHF-tau in ROS/MAP were tested for their association with CSF T-tau and P-tau levels in ADNI. 2286 and 2330 SNP-SNP interactions were validated by T-tau and P-tau, respectively (Table 2). Among them, 270 and 294 SNP-SNP interactions which were significant under Bonferroni correction in ROS/MAP were validated by T-tau and P-tau, respectively (Supplemental Tables S1 and S2). There are 1813 SNP-SNP interactions validated by both T-tau and P-tau and 2803 SNP-SNP interactions validated by either T-tau or P-tau (Table 2), conforming with the high correlation between T-tau and P-tau levels ( $R^2 = 0.98$ , see Supplementary Fig. S1).

For neuritic plaques, diffuse plaques, and total amyloid, a total of 305,415, 337,902, and 305,302 SNP-SNP interactions met the criterion of a cell size either more than 3 or equal to 0 and a nominal  $P$  threshold of  $1 \times 10^{-5}$  in the first stage. 3980 (neuritic plaques), 10,931 (diffuse plaques), and 3816 (total amyloid) suggestive SNP-SNP interactions were reported by genotypic model. Among them, 47 (neuritic plaques), 212 (diffuse plaques), and 20 (total

amyloid) SNP-SNP interactions were significant under a Bonferroni-based nominal threshold of  $3.98 \times 10^{-12}$ . For validation, candidate SNP-SNP interactions discovered for neuritic plaques, diffuse plaques, and total amyloid in ROS/MAP were tested for their association with CSF  $A\beta_{1-42}$  levels in ADNI, resulting in 464 SNP-SNP interactions being validated after filtering out spurious interactions caused by long-range LD (Table 2). Among them, 11 SNP-SNP interactions which were significant under Bonferroni correction in ROS/MAP were validated (Supplemental Table S3).

Overall, we obtained 2803 and 464 validated SNP-SNP interactions for tau and  $A\beta$  neuropathology, respectively (Supplementary Table S1–S3). Interestingly and unexpected, there was no overlap between identified SNP-SNP interactions for the 2 AD hallmarks.

### 3.2. Functional annotations for candidate interactions

To gain an overview of the functional consequences of the candidate SNP-SNP interactions, we mapped the identified SNPs onto the genome. We found that most SNPs fall on the distal intergenic regions or introns (Fig. S2), which highlights the possible function of “junk DNA” in genetic regulation. As reported in a previous study, the brain has distinct expression and epigenetic patterns, including a greater extent of noncoding transcription than other tissues (Gandal et al., 2018).

Moreover, the enriched gene ontology (GO) terms, KEGG pathways and Reactome (Yu et al., 2012; Yu and He, 2016), for genes mapped by these SNPs were examined. First, we examined the genes related to tau pathology; 7 of the top 10 enriched biological processes in GOs were related to the nervous system, such as negative regulation of neuron differentiation, axon development, and axonogenesis (Fig. 2A). Pathway analysis shows enrichment of genes in neuroactive ligand-receptor interaction, cAMP signaling pathway, and various other pathways (Fig. S3). The most

**Table 2**  
ROS/MAP stage1 and stage2, as well as ADNI1/GO/2 replicated SNP-SNP interactions

ROS/MAP Phenotype	ROS/MAP		ADNI	
	First stage	Second stage	Phenotype	Validation
Neurofibrillary tangles	435,358	32,960	CSF T-tau/P-tau	2286/2330 (2803)
Total PHF-tau	526,204	65,263		
Neuritic plaques	305,415	3980	CSF $A\beta_{1-42}$	464
Diffuse plaques	337,902	10,931		
Total amyloid	305,302	3816		

Key: AD, Alzheimer's disease; ADNI, Alzheimer's Disease Neuroimaging Initiative; PHF-tau, paired helical filament tau; ROS/MAP, The Religious Orders Study/the Rush Memory and Aging Project.

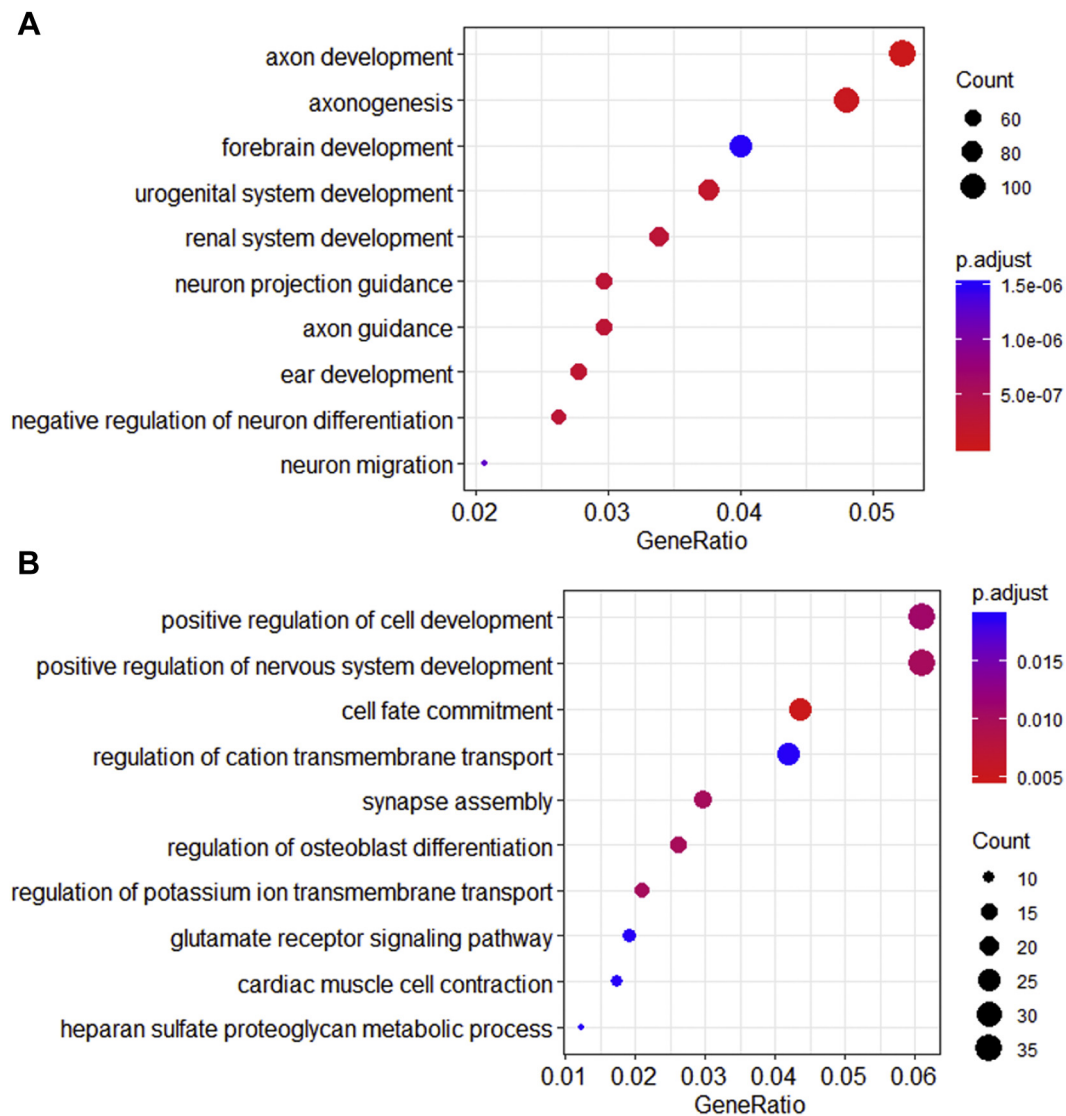


**Fig. 2.** Functional annotation of SNPs identified by tau-related pathology and A $\beta$ -related pathology. (A) For tau-related pathology, top 10 biological processes identified by gene ontology enrichment analysis for genes mapped by the identified SNPs. (B) For A $\beta$ -related pathology, top 10 biological processes identified by gene ontology enrichment analysis for genes mapped by the identified SNPs. Abbreviation: A $\beta$ , amyloid- $\beta$ .

significantly enriched pathway was neuroactive ligand-receptor interaction, which was already found to be related to analgesic, anticonvulsant, and repair reduction of cholinergic neurons and the secretion of neurotoxic inflammatory cytokine related to AD (Liu et al., 2019). As for cAMP signaling pathway, it has important roles in the long-term potentiation and is a promising drug targetable pathways for AD (Fiorito et al., 2018; Vitolo et al., 2002).

Next, we examined the genes mapped by interacting SNPs for A $\beta$  pathology. GO analysis showed that various biological processes including positive regulation of nervous system development, glutamate receptor signaling pathway, and regulation of cation transmembrane transport were enriched (Fig. 2B). Pathway analysis shows the enrichment of 2 pathways: neuronal system and deleted in colorectal carcinoma (DCC)-mediated attractive signaling. Interestingly, amyloid precursor protein functionally acts as a co-receptor for DCC to mediate axon guidance (Rama et al., 2012). More specifically, amyloid precursor protein interacts with DCC in the presence of netrin-1 and enhances netrin-1-mediated DCC intracellular signaling, such as MAPK activation (Rama et al., 2012).

In summary, the functional consequences of the candidate interactions for tau and A $\beta$  neuropathology are tightly connected to the relevant GO terms or pathways, thereby providing robust support for their involvement in AD.

### 3.3. Transcriptome analysis of candidate interactions

The expression levels of 2 interacting genes are frequently co-altered (Wang et al., 2014). Therefore, we performed a co-expression analysis of interacting gene pairs. There are 2803 validated SNP-SNP interactions identified using tau pathology. After SNPs were mapped to the corresponding genes, there are 1195 gene pairs retained for co-expression analysis. Of 1195 interacting gene pairs, 522 gene pairs showed significant co-expression under a Bonferroni-corrected  $p$  value of 0.05 (793 gene pairs were significant under a nominal  $p$  value of 0.05) (Supplementary Table S4). *MAPK9* which was previously associated with T-tau, P-tau, and neurofibrillary AD pathology (Kim et al., 2015) and *OPCML* which showed significant differential expression in patients with AD

(Zelaya et al., 2015) was the most significantly co-expressed gene pair ( $R^2 = 0.93$ ,  $P_{nominal} = 6.33 \times 10^{-241}$ ). Particularly, *MAPK9* also showed interaction and high correlation with *CAMKK1* ( $R^2 = 0.83$ ,  $P_{nominal} = 6.66 \times 10^{-140}$ ), which was involved in the phosphorylation of tau protein by activation of calcium/calmodulin-dependent protein kinase IV (Ye et al., 2017). Therefore, the role of *MAPK9* in tau-related AD pathology is worth a further experimental validation. Moreover, the interaction between *GRIN2A* and *EPHA4* ( $R^2 = 0.88$ ,  $P_{nominal} = 1.67 \times 10^{-175}$ ) was ranked in the second place by co-expression, providing promising drug targets for the treatment of AD. *GRIN2A* encodes a subunit of N-methyl-D-aspartate receptor, which is inhibited by several FDA-approved drugs for treatment of AD (Olivares et al., 2012). Meanwhile, EphA4 protein has been suggested as potential drug target for AD (Gu et al., 2018), and blockade of EphA4 signaling ameliorates synaptic dysfunctions in mouse models of AD (Fu et al., 2014). *TENM3* and *TLN2* ( $R^2 = 0.88$ ,  $P_{nominal} = 3.73 \times 10^{-175}$ ), whose interaction was ranked in the third place by co-expression, have both been associated with AD in a sex specific manner (Deming et al., 2018; Gusareva et al., 2018), indicating the complex interplay between sex and genetic background regarding AD predisposition.

Regarding A $\beta$  neuropathology, of 179 gene pairs meeting the selection criterion, 81 gene pairs were co-expressed in the brain with a Bonferroni-corrected  $P$  smaller than 0.05 (111 gene pairs with  $P_{nominal} < 0.05$ ) (Supplementary Table S5). *INPP4B* and *RBFOX1* was the most significantly co-expressed gene pair ( $R^2 = 0.83$ ,  $P_{nominal} = 7.10 \times 10^{-140}$ ). *RBFOX1* encodes proteins that can regulate alternative splicing events. Downregulation of *RBFOX1* leads to destabilization of mRNAs encoding for synaptic transmission proteins, which contribute to the loss of synaptic function in AD (Alkallal et al., 2017). Interestingly, *INPP4B* was 5-fold lower expressed in lymphoblastoid cells lines exhibiting high A $\beta$  sensitivity (Hadar et al., 2016), conforming with the downregulation of *RBFOX1* in AD. *CSMD1* and *SLC16A14* ( $R^2 = 0.74$ ,  $P_{nominal} = 2.20 \times 10^{-94}$ ), whose interaction was ranked in the second place by co-expression, were both associated to cognitive functions (Athanasou et al., 2017; Fisel et al., 2018). Gene-gene interactions that were validated by co-expression with a

$P_{nominal} < 0.05$  for A $\beta$  and tau are displayed in Supplementary Tables S4 and S5, respectively.

#### 3.4. Candidate interactions and in vivo neuroimaging

To discovery possible implications of the AD pathology on brain damage, we tested the association of candidate interactions with brain atrophy and white matter injury. Specifically, the SNP-SNP interactions of tau and A $\beta$  neuropathology were analyzed for their association with entorhinal cortex volume, hippocampal volume, and estimates of FA across 5 regions using data derived from in vivo neuroimaging. There are no significant SNP-SNP interactions for entorhinal cortex volume and hippocampal volume after adjusting for multiple tests.

However, one SNP-SNP interaction associated with tau neuropathology in ROS/MAP and ANDI was also associated with FA estimates after adjusting for multiple tests. Specifically, the interaction between rs2189344 and rs777307 was associated with FA estimates in splenium of corpus callosum (left,  $P_{nominal} = 1.40 \times 10^{-4}$ ; right  $P_{nominal} = 3.37 \times 10^{-6}$ ). Individuals with TT genotype in rs2189344 and GG genotype in rs777307 showed higher total PHF-tau in the brain, higher CSF T-tau levels, and lower FA estimates in splenium of corpus callosum (Fig. 3).

The rs2189344 is in the intron of *AC004538.3*, which encodes several antisense RNAs. The rs777307 is in the intron of *AC072062.1*, which encodes long noncoding RNAs. Leveraging expression quantitative trait loci (eQTLs) in the genotype tissue expression project database (Lonsdale et al., 2013), we found that rs2189344 was a significant eQTL of *AC004538.3* ( $P_{nominal} = 3.1 \times 10^{-5}$ ) and rs777307 was also a significant eQTL of *AC072062.1* ( $P_{nominal} = 1.6 \times 10^{-8}$ ). Together, the interaction indicates the important role of noncoding RNAs in AD pathology and supports the association between tau pathology and white matter damage (Amlien and Fjell, 2014). Moreover, this result further shows the involvement of white matter in AD, which has been traditionally considered as a gray matter disease.

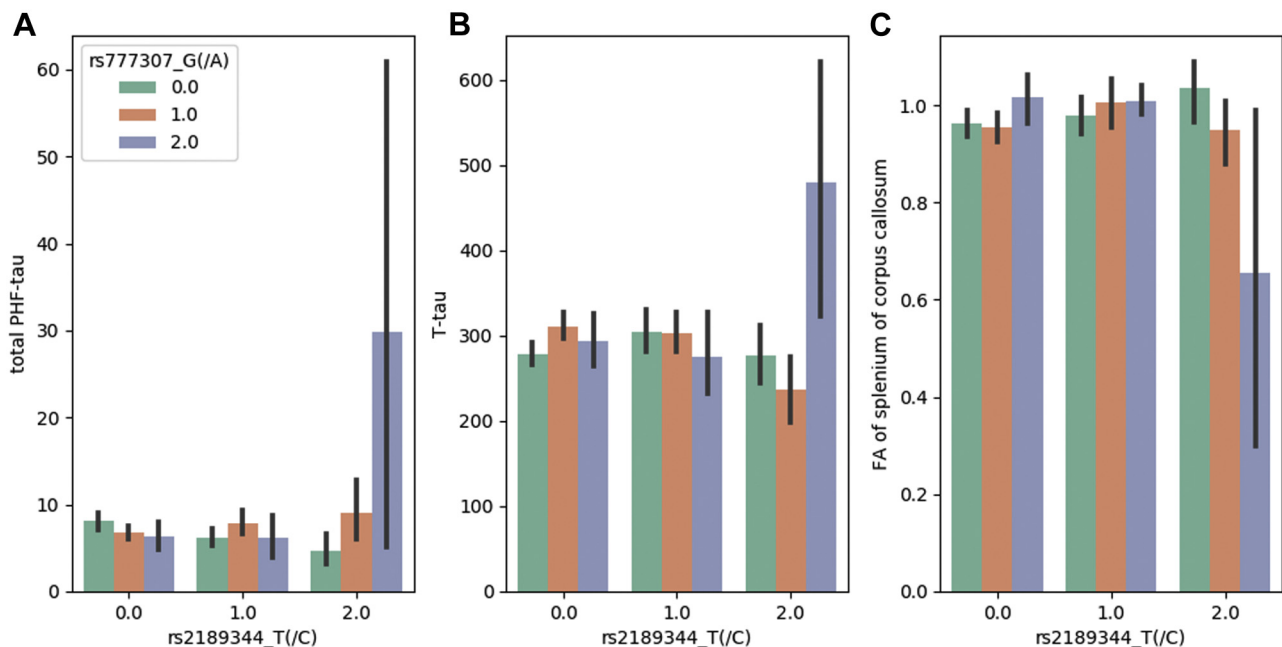


**Fig. 3.** The interaction effects of rs2189344 and rs777307 on total PHF-tau, CSF T-tau, and fractional anisotropy (FA) estimates of splenium of corpus callosum. (A) The interaction effect of rs2189344 and rs777307 on total PHF-tau. (B) The interaction effect of rs2189344 and rs777307 on CSF T-tau. (C) The interaction effect of rs2189344 and rs777307 on FA estimates of splenium of corpus callosum. The mean value of each measurement is plotted against each pairwise genotype combination of rs2189344 and rs777307. The error bar indicates standard deviation. Abbreviation: PHF-tau, paired helical filament tau.

#### 4. Discussion

Tau and A $\beta$  neuropathology are the 2 neuropathological hallmarks of AD (Tapiola et al., 2009). Therefore, we conducted a genome-wide epistasis analysis of these 2 pathologies in post-mortem brain in ROS/MAP and validated the discovery using CSF biomarkers of AD in ADNI. As a result, we identified 2803 and 464 candidate interactions for tau and A $\beta$  neuropathology, respectively. Next, the functional consequences of the candidate SNP-SNP interactions were examined. We found that most SNPs are on the distal intergenic regions or introns, which is in accordance with the assumed regulatory function of epistasis. GO terms and pathways related to the nervous system were enriched by the genes mapped by the SNPs, providing additional validation of candidate interactions.

Here, we mapped an SNP to genes only by its genomic position. Ideally, regulatory information such as eQTLs and 3D proximity obtained by chromosome conformation capture-based approaches can be used to map an SNP to its corresponding genes. However, one SNP could be mapped to dozens of genes after incorporating eQTL and 3D proximity. As a result, for one SNP-SNP interaction, it could be mapped to hundreds of gene pairs, which would lead to confusions in downstream analysis. Consequently, in this study, only the genomic position was considered when mapping an SNP to genes.

After SNP-SNP interactions were mapped into gene-gene interactions, we ranked gene pairs according to their co-expression in the brain, therefore providing a ranked list for further examination. For tau neuropathology, 793 of 1195 gene pairs were supported by their significant co-expression. For A $\beta$  neuropathology, 111 of 179 gene pairs were supported by their significant co-expression. These gene-gene interactions provide a valuable resource for further exploration of disease mechanisms and discovery of new drugs. For example, several interactions including *MAPK9-CAMKK1* and *GRIN2A-EPHA4* are involved in Ca<sup>2+</sup>-mediated signaling function (Corrigan et al., 2005), providing new evidences for the disruption of cellular calcium homeostasis in AD. Furthermore, these gene-gene interactions can be promising drug targets after functional validation, as partially inhibition of several targets can be more efficient than complete inhibition of a single target (Csermely et al., 2005).

In addition, SNP-SNP interactions identified were tested for their association with brain atrophy and white matter injury. However, no significant SNP-SNP interaction was found for entorhinal cortex volume and hippocampal volume after adjusting for multiple tests, which may be caused by the lack of statistical power due to small sample sizes. One SNP-SNP interaction, rs2189344 and rs777307, was associated with FA estimates in splenium of corpus callosum, suggesting the association between tau neuropathology and white matter damage. The biological mechanisms of the SNP-SNP interaction warrant further experimental validation.

We also tested the association of candidate SNP-SNP interactions with diagnosis of Alzheimer's dementia. Interestingly, only 4 of the 464 interaction for A $\beta$  neuropathology and 49 of 2803 interactions for tau neuropathology are significantly associated with Alzheimer's dementia in both ROS/MAP and ADNI, conforming to the fact that tau and A $\beta$  neuropathology may be found in individuals with or without a diagnosis of Alzheimer's dementia. It also indicates that tau and A $\beta$  neuropathology alone may be insufficient for the development of Alzheimer's dementia.

Overconservative *p* value threshold caused by Bonferroni correction can lead to high false negative rate (high type II error) (White et al., 2019). To alleviate this problem, we also reported SNP-SNP interactions as “suggestive” that passed a less conservative correction accounting for the number of tests performed in the

second stage of our analysis. To reduce possible false positives, independent replication cohorts were used to validate the SNP-SNP interactions identified by the 2-stage analysis. And further investigations are required for interactions that are suggestive of (but not reaching) significance.

Statistically significant epistasis is not necessarily a biologically meaningful interaction. Statistical epistasis represents the departure from a specific linear model describing the relationship between the alleles at different loci with respect to their contribution to a phenotype (Cordell, 2002). However, biological inferences from statistical epistasis require prior knowledge of the specific alleles involved. Here, we attempted to partially interpret statistical epistasis by visualizing each cell in the 3 × 3 two-locus genotype combination. Another limitation of statistical epistasis is that statistical models can be incredible when there are cells with very few samples in the 3 × 3 two-locus genotype table, which often leads to misleading significant interactions by regression methods. We alleviated this problem by excluding pairs with a cell size smaller than 3 in any cell of the 3 × 3 contingency table.

#### Disclosure statement

The authors have no actual or potential conflicts of interest. No author's institution has contracts relating to this research through which it or any other organization may stand to gain financially now or in the future. No other agreements of authors or their institutions that could be seen as involving a financial interest in this work.

#### CRediT authorship contribution statement

**Hui Wang:** Investigation, Writing - review & editing. **Jingyun Yang:** Validation, Writing - review & editing. **Julie A. Schneider:** Validation, Writing - review & editing. **Philip L. De Jager:** Validation, Writing - review & editing. **David A. Bennett:** Validation, Writing - review & editing. **Hong-Yu Zhang:** Conceptualization, Writing - review & editing.

#### Acknowledgements

This work was supported by the Fundamental Research Funds for the Central Universities (Grant 2662017PY115).

Work from Rush was supported in part by grants P30AG10161, R01AG15819, R01AG17917, U01AG61356, R01AG30146, the Illinois Department of Public Health, and the Translational Genomics Research Institute (Kronos Science). The authors are indebted to the participants in the Religious and the Orders Study and the Rush Memory and Aging Project.

Data obtained from the Alzheimer's Disease Neuroimaging Initiative (ADNI) database were funded by the Alzheimer's Disease Neuroimaging Initiative (ADNI) (National Institutes of Health Grant U01 AG024904) and DOD ADNI (Department of Defense award number W81XWH-12-2-0012). The investigators within the ADNI contributed to the design and implementation of ADNI and/or provided data but did not participate in analysis or writing of this report.

#### Appendix A. Supplementary data

Supplementary data to this article can be found online at <https://doi.org/10.1016/j.neurobiolaging.2020.04.025>.

## References

- Alkallas, R., Fish, L., Goodarzi, H., Najafabadi, H.S., 2017. Inference of RNA decay rate from transcriptional profiling highlights the regulatory programs of Alzheimer's disease. *Nat. Commun.* 8, 909.
- Amlien, I.K., Fjell, A.M., 2014. Diffusion tensor imaging of white matter degeneration in Alzheimer's disease and mild cognitive impairment. *Neuroscience* 276, 206–215.
- Athanasiu, L., Giddaluru, S., Fernandes, C., Christoforou, A., Reinvang, I., Lundervold, A.J., Nilsson, L.-G., Kauppi, K., Adolfsson, R., Eriksson, E., 2017. A genetic association study of CSMD1 and CSMD2 with cognitive function. *Brain Behav. Immun.* 61, 209–216.
- Bennett, D.A., Buchman, A.S., Boyle, P.A., Barnes, L.L., Wilson, R.S., Schneider, J.A., 2018. Religious Orders study and Rush memory and aging project. *J. Alzheimers Dis.* 64, S161–S189.
- Bennett, D.A., De Jager, P.L., Leurgans, S.E., Schneider, J.A., 2009. Neuropathologic intermediate phenotypes enhance association to Alzheimer susceptibility alleles. *Neurology* 72, 1495–1503.
- Casper, J., Zweig, A.S., Villarreal, C., Tyner, C., Speir, M.L., Rosenbloom, K.R., Raney, B.J., Lee, C.M., Lee, B.T., Karolchik, D., 2017. The UCSC genome browser database: 2018 update. *Nucleic Acids Res.* 46, D762–D769.
- Chang, C.C., Chow, C.C., Tellier, L.C., Vattikuti, S., Purcell, S.M., Lee, J.J., 2015. Second-generation PLINK: rising to the challenge of larger and richer datasets. *GigaScience* 4, 7.
- Combarros, O., Cortina-Borja, M., Smith, A.D., Lehmann, D.J., 2009a. Epistasis in sporadic Alzheimer's disease. *Neurobiol. Aging* 30, 1333–1349.
- Combarros, O., van Duijn, C.M., Hammond, N., Belbin, O., Arias-Vásquez, A., Cortina-Borja, M., Lehmann, M.G., Aulchenko, Y.S., Schuur, M., Kölsch, H., 2009b. Replication by the Epistasis Project of the interaction between the genes for IL-6 and IL-10 in the risk of Alzheimer's disease. *J. Neuroinflammation* 6, 22.
- Consortium, G.P., Auton, A., Brooks, L.D., 2015. A global reference for human genetic variation. *Nature* 526, 68–74.
- Cordell, H.J., 2002. Epistasis: what it means, what it doesn't mean, and statistical methods to detect it in humans. *Hum. Mol. Genet.* 11, 2463–2468.
- Corrigan, C., Subramanian, R., Miller, M.A., 2005. Eph and NMDA receptors control Ca<sup>2+</sup>/calmodulin-dependent protein kinase II activation during C. elegans oocyte meiotic maturation. *Development* 132, 5225–5237.
- Csermely, P., Agoston, V., Pongor, S., 2005. The efficiency of multi-target drugs: the network approach might help drug design. *Trends Pharmacol. Sci.* 26, 178–182.
- Das, S., Forer, L., Schönherr, S., Sidore, C., Locke, A.E., Kwong, A., Vrieze, S.I., Chew, E.Y., Levy, S., McGue, M., 2016. Next-generation genotype imputation service and methods. *Nat. Genet.* 48, 1284.
- Deming, Y., Dumitrescu, L., Barnes, L.L., Thambisetty, M., Kunkle, B., Gifford, K.A., Bush, W.S., Chibnik, L.B., Mukherjee, S., De Jager, P.L., 2018. Sex-specific genetic predictors of Alzheimer's disease biomarkers. *Acta Neuropathol.* 136, 857–872.
- Fiorito, J., Deng, S.-X., Landry, D.W., Arancio, O., 2018. Targeting the NO/cGMP/CREB phosphorylation signaling pathway in Alzheimer's disease. In: *Neurochemical Basis of Brain Function and Dysfunction*. IntechOpen, London, UK.
- Fisel, P., Schaeffeler, E., Schwab, M., 2018. Clinical and functional relevance of the monocarboxylate transporter family in disease pathophysiology and drug therapy. *Clin. translational Sci.* 11, 352–364.
- Fu, A.K., Hung, K.-W., Huang, H., Gu, S., Shen, Y., Cheng, E.Y., Ip, F.C., Huang, X., Fu, W.-Y., Ip, N.Y., 2014. Blockade of EphA4 signaling ameliorates hippocampal synaptic dysfunctions in mouse models of Alzheimer's disease. *Proc. Natl. Acad. Sci.* 111, 9959–9964.
- Gandal, M.J., Zhang, P., Hadjimichael, E., Walker, R.L., Chen, C., Liu, S., Won, H., van Bakel, H., Varghese, M., Wang, Y., 2018. Transcriptome-wide isoform-level dysregulation in ASD, schizophrenia, and bipolar disorder. *Science* 362, eaat8127.
- Gatz, M., Reynolds, C.A., Fratiglioni, L., Johansson, B., Mortimer, J.A., Berg, S., Fiske, A., Pedersen, N.L., 2006. Role of genes and environments for explaining Alzheimer disease. *Arch. Gen. Psychiatry* 63, 168–174.
- Gu, S., Fu, W.-Y., Fu, A.K., Tong, E.P.S., Ip, F.C., Huang, X., Ip, N.Y., 2018. Identification of new EphA4 inhibitors by virtual screening of FDA-approved drugs. *Scientific Rep.* 8, 7377.
- Gusareva, E.S., Carrasquillo, M.M., Bellenguez, C., Cuyvers, E., Colon, S., Graff-Radford, N.R., Petersen, R.C., Dickson, D.W., John, J.M.M., Bessonov, K., 2014. Genome-wide association interaction analysis for Alzheimer's disease. *Neurobiol. Aging* 35, 2436–2443.
- Gusareva, E.S., Twizere, J.-C., Slegers, K., Dourlen, P., Abisambra, J.F., Meier, S., Cloyd, R., Weiss, B., Dermaut, B., Bessonov, K., 2018. Male-specific epistasis between WWC1 and TLN2 genes is associated with Alzheimer's disease. *Neurobiol. Aging* 72, 188.e3–188.e12.
- Hadar, A., Milanesi, E., Squassina, A., Niola, P., Chillotti, C., Pasmanik-Chor, M., Yaron, O., Martásek, P., Rehavi, M., Weissglas-Volkov, D., 2016. RGS2 expression predicts amyloid- $\beta$  sensitivity, MCI and Alzheimer's disease: genome-wide transcriptomic profiling and bioinformatics data mining. *Transl. Psychiatry* 6, e909.
- Herold, C., Steffens, M., Brockschmidt, F.F., Baur, M.P., Becker, T., 2009. INTERSNP: genome-wide interaction analysis guided by a priori information. *Bioinformatics* 25, 3275–3281.
- Kauwe, J.S.K., Bertelsen, S., Mayo, K., Cruchaga, C., Abraham, R., Hollingsworth, P., Harold, D., Owen, M.J., Williams, J., Lovestone, S., 2010. Suggestive synergy between genetic variants in TF and HFE as risk factors for Alzheimer's disease. *Am. J. Med. Genet. B: Neuropsychiatr. Genet.* 153, 955–959.
- Kim, S., Nho, K., Risacher, S.L., Shen, L., Shaw, L.M., Trojanowski, J.Q., Weiner, M.W., Saykin, A.J., 2015. Map2 as a novel Alzheimer's disease target gene from gwas of CSF amyloid beta 1–42, tau and hyperphosphorylated tau in the ADNI cohort. *Alzheimers Dement.* 11, P767–P768.
- Lambert, J.-C., Ibrahim-Verbaas, C.A., Harold, D., Naj, A.C., Sims, R., Bellenguez, C., Jun, G., DeStefano, A.L., Bis, J.C., Beecham, G.W., 2013. Meta-analysis of 74,046 individuals identifies 11 new susceptibility loci for Alzheimer's disease. *Nat. Genet.* 45, 1452.
- Lee, S.H., Harold, D., Nyholt, D.R., ANZGene Consortium, International Endogene Consortium, Genetic and Environmental Risk for Alzheimer's disease Consortium, Goddard, M.E., Zondervan, K.T., Williams, J., Montgomery, G.W., Wray, N.R., Visscher, P.M., 2013. Estimation and partitioning of polygenic variation captured by common SNPs for Alzheimer's disease, multiple sclerosis and endometriosis. *Hum. Mol. Genet.* 22, 832–841.
- Liu, J., Hu, A., Zan, J., Wang, P., You, Q., Tan, A., 2019. Network Pharmacology Deciphering mechanisms of Volatiles of Wendan Granule for the treatment of Alzheimer's disease. *Evid. Based Complement. Alternat. Med.* 2019, 7826769.
- Loh, P.-R., Danecek, P., Palamara, P.F., Fuchsberger, C., Reshef, Y.A., Finucane, H.K., Schoenherr, S., Forer, L., McCarthy, S., Abecasis, G.R., 2016. Reference-based phasing using the haplotype reference Consortium panel. *Nat. Genet.* 48, 1443.
- Lonsdale, J., Thomas, J., Salvatore, M., Phillips, R., Lo, E., Shad, S., Hasz, R., Walters, G., Garcia, F., Young, N., 2013. The genotype-tissue expression (GTEx) project. *Nat. Genet.* 45, 580.
- Murk, W., DeWan, A.T., 2016. Exhaustive genome-wide search for SNP-SNP interactions across 10 human diseases. *G3 (Bethesda)* 6, 2043–2050.
- Olivares, D., K Deshpande, V., Shi, Y., K Lahiri, D., H Greig, N., T Rogers, J., Huang, X., 2012. N-methyl D-aspartate (NMDA) receptor antagonists and memantine treatment for Alzheimer's disease, vascular dementia and Parkinson's disease. *Curr. Alzheimer Res.* 9, 746–758.
- Petersen, R.C., Aisen, P.S., Beckett, L.A., Donohue, M.C., Gamst, A.C., Harvey, D.J., Jack, C.R., Jagust, W.J., Shaw, L.M., Toga, A.W., 2010. Alzheimer's disease neuroimaging initiative (ADNI): clinical characterization. *Neurology* 74, 201–209.
- Raghavan, N., Tosto, G., 2017. Genetics of Alzheimer's disease: the importance of polygenic and epistatic components. *Curr. Neurol. Neurosci. Rep.* 17, 78.
- Rama, N., Goldschneider, D., Corset, V., Lambert, J., Pays, L., Mehlen, P., 2012. Amyloid precursor protein regulates netrin-1-mediated commissural axon outgrowth. *J. Biol. Chem.* 287, 30014–30023.
- Remarque, E.J., Bollen, E., Weverling-Rijnsburger, A.W.E., Laterveer, J.C., Blauw, G.J., Westendorp, R.G.J., 2001. Patients with Alzheimer's disease display a pro-inflammatory phenotype. *Exp. Gerontol.* 36, 171–176.
- Ridge, P.G., Mukherjee, S., Crane, P.K., Kauwe, J.S.K., 2013. Alzheimer's disease: Analyzing the missing heritability. *PLoS One* 8, e79771.
- Robson, K.J.H., Lehmann, D.J., Wimhurst, V.L.C., Livesey, K.J., Combrinck, M., Merriweather-Clarke, A.T., Warden, D.R., Smith, A.D., 2004. Synergy between the C2 allele of transferrin and the C282Y allele of the haemochromatosis gene (HFE) as risk factors for developing Alzheimer's disease. *J. Med. Genet.* 41, 261–265.
- Tanzi, R.E., 2012. The genetics of Alzheimer disease. *Cold Spring Harbor Perspect. Med.* 2, a006296.
- Tapiola, T., Alafuzoff, I., Herukka, S.-K., Parkkinen, L., Hartikainen, P., Soininen, H., Pirttilä, T., 2009. Cerebrospinal fluid  $\beta$ -amyloid 42 and tau proteins as biomarkers of Alzheimer-type pathologic changes in the brain. *Arch. Neurol.* 66, 382–389.
- Van Leeuwen, E.M., Kanterakis, A., Deelen, P., Kattenberg, M.V., Abdellaoui, A., Hofman, A., Schönhuth, A., Menelaou, A., de Craen, A.J., van Schaik, B.D., 2015. Population-specific genotype imputations using minimac or IMPUTE2. *Nat. Protoc.* 10, 1285.
- Vitolo, O.V., Sant'Angelo, A., Costanzo, V., Battaglia, F., Arancio, O., Shelanski, M., 2002. Amyloid  $\beta$ -peptide inhibition of the PKA/CREB pathway and long-term potentiation: reversibility by drugs that enhance cAMP signaling. *Proc. Natl. Acad. Sci.* 99, 13217–13221.
- Wan, X., Yang, C., Yang, Q., Xue, H., Fan, X., Tang, N.L., Yu, W., 2010. BOOST: a fast approach to detecting gene-gene interactions in genome-wide case-control studies. *Am. J. Hum. Genet.* 87, 325–340.
- Wang, X., Fu, A.Q., Mc Nerney, M.E., White, K.P., 2014. Widespread genetic epistasis among cancer genes. *Nat. Commun.* 5, 4828.
- White, T., van der Ende, J., Nichols, T.E., 2019. Beyond bonferroni revisited: concerns over inflated false positive research findings in the fields of conservation genetics, biology, and medicine. *Conservation Genet.* 1–11.
- Ye, S., Wang, T., Cai, B., Wang, Y., Li, J., Zhan, J., Shen, G., 2017. Genistein protects hippocampal neurons against injury by regulating calcium/calmodulin dependent protein kinase IV protein levels in Alzheimer's disease model rats. *Neural Regen. Res.* 12, 1479.
- Yu, G., He, Q.-Y., 2016. ReactomePA: an R/Bioconductor package for reactome pathway analysis and visualization. *Mol. BioSystems* 12, 477–479.
- Yu, G., Wang, L.-G., Han, Y., He, Q.-Y., 2012. clusterProfiler: an R package for comparing biological themes among gene clusters. *OMICS* 16, 284–287.
- Zelaya, M.V., Pérez-Valderrama, E., de Morentin, X.M., Tuñón, T., Ferrer, I., Luquin, M.R., Fernandez-Irigoyen, J., Santamaría, E., 2015. Olfactory bulb proteome dynamics during the progression of sporadic Alzheimer's disease: identification of common and distinct olfactory targets across Alzheimer-related co-pathologies. *Oncotarget* 6, 39437.